

Europa's Hemispheric Color Dichotomy as a Constraint on Non-synchronous Rotation

Ethan Burnett* and Paul Hayne†

Europa's surface reflectance exhibits a pronounced hemispheric dichotomy, which is hypothesized to form due to enhanced irradiation of the trailing hemisphere by energetic particles entrained in the jovian magnetosphere. We propose that this pattern can only persist if the timescale for discoloration is much shorter than that of Europa's rotation relative to the synchronous state. By decomposing the longitudinal ultraviolet and visible color variations from Voyager data into sine and cosine terms, we demonstrate that the contribution due to non-synchronous rotation is small. The results of this analysis suggest that there is essentially no non-synchronous rotation of Europa on geologic timescales, with the period of non-synchronous rotation > 1 Gyr. This same conclusion is reached with two models of discoloration: one representing an actively discoloring surface, and the other assuming that the present-day exogenic discoloration on the surface is in steady-state. This constraint depends on the age of the crater Pwyll, which is assumed to be $\sim 10^6$ yr; an older age would indicate a slower non-synchronous rotation period. This result magnifies the outstanding problem of generating sufficient stress to explain Europa's pervasive tectonic features.

1 Introduction

The present-day icy surface of Europa is covered with large ridges and cracks, which are generally the result of tidal stresses during Europa's eccentric 3.55-day orbit about Jupiter. Tectonic models of surface cracks are only poorly constrained by observational data, primarily due to uncertainty in the thickness of Europa's ice shell, with most studies predicting thickness orders ranging from several kilometers up to tens of kilometers [7, 21]. Some surface features are not well explained by the stress field predicted to arise from the diurnal variations in tidal forces alone. In particular, the work of Hoppa [12] and Greenberg et al. [8, 9] suggests the existence of a large background stress field, which they attribute to slow non-synchronous rotation from Europa's tidally locked orientation. [9] Additionally, analysis by Katterhorn et al. [17] and Geissler et al. [4] also interpreted tectonic features as evidence for non-synchronous rotation. However, direct evidence of non-synchronous rotation is lacking, due to both the timescale of the hypothesized asynchronicity and the limitations of available data. Alternative models suggest that the background stress field could be due to polar wander, [8] which has support from several theoretical and observational studies. [22, 23, 26]

Another salient feature of Europa's surface is the hemispheric color asymmetry, likely due to interactions between the surface and the Jovian magnetosphere [3]. Such irradiation patterns also appear to be common among the icy saturnian satellites. [13] Multispectral studies reveal a

*Aerospace Engineering Sciences, University of Colorado Boulder, ethan.burnett@colorado.edu

†Astrophysical and Planetary Sciences, University of Colorado Boulder, paul.hayne@colorado.edu

global asymmetry in albedo and color between the leading and trailing hemispheres, particularly in the relative ultraviolet (UV) spectral reflectance. [18] Several studies have attributed the global hemispheric color asymmetry to an exogenic process. [19, 20] The primary goal of this work is to investigate whether exogenous patterns in the color distribution of Europa’s surface are consistent with non-synchronous rotation.



Figure 1: Europa Color Map (Albers)

2 Europa’s Rotation State and Stress Field

2.1 Orbit and Rotation

The orbits of Io, Europa, and Ganymede are in a resonant configuration such that their mean motions are commensurate in a 4:2:1 ratio. Writing ν_i as the mean longitude of the i th satellite, the moons Io (1), Europa (2), and Ganymede (3) satisfy the following relationship:

$$\nu_1 - 3\nu_2 + 2\nu_3 \approx \pi \quad (1)$$

This relationship is commonly referred to as the Laplace resonance. The configuration is believed to have resulted from outward migration of the orbits of the three moons due to tidal dissipation. [5] Tidal dissipation is also the source of the energy that feeds the volcanism on Io and sustains the liquid subsurface ocean on Europa. The 4:2:1 resonance also forces Europa’s orbit to maintain an eccentricity of $e \approx 0.01$, and this eccentricity results in variations in the tidal force due to Jupiter, resulting in periodic changes in the stress field acting on the entire body, including the surface ice.

Europa’s slightly eccentric orbit could result in non-synchronous rotation. This is because for an eccentric orbit, the orbit-averaged tidal torque vanishes for a body angular velocity that is slightly above synchronous. Because the maximum tidal torque occurs at periapsis, the tides can force the spin to be synchronized with the orbit angular velocity at periapsis. [25]

However, in the presence of sufficiently large permanent mass asymmetries, the gravitational torque on these asymmetries will tend to force spins that are half-integer multiples of the orbital mean motion, for which synchronous rotation is most typical. For an asymmetric body with rotation axis aligned with the orbit angular momentum, the condition for the average tidal torque τ to overcome the tendency for synchronous rotation is given as: [6]

$$\tau > \frac{3}{2}(B - A) \left(1 - \frac{5}{2}e^2\right) n^2 \quad (2)$$

where e is the orbit eccentricity, n is the orbital mean motion, and A and B are the moments of inertia in the equatorial plane, with $B > A$. If the average tidal torque τ is above this critical value, it would suggest the possibility of the existence of non-synchronous rotation, whereas a much smaller value would suggest dynamical conditions favoring synchronous rotation. It is not known with certainty that Europa has sufficient mass asymmetry to enforce synchronous rotation. Even if Europa’s mantle retains sufficient asymmetry for this to be the case, it is possible that the ice shell on Europa is still in a non-synchronous rotation state due to the decoupling of the icy shell from the interior by the inviscid subsurface ocean. [9]

2.2 Tectonic Features as Evidence for Non-synchronous Rotation

Cycloidal fractures are prominent on Europa’s surface, such as those shown in the high-resolution Galileo images in Figure 2. [12] These features exhibit similar morphology to so-called ‘double-ridges’, which are the most common tectonic features on Europa. [12] Hoppa and Greenberg pro-



Figure 2: Cycloidal Double Ridges on Europa [12]

posed that the cycloidal features form as tension cracks in the ice, with the distinct shape being due to crack propagation through a diurnally varying stress field. [8, 12] In their model, a crack forms perpendicular to the local direction of maximum tensile stress and begins to propagate, following a curving path due to the changing orientation of the stress field. The stops between arcs are hypothesized to be due to the tensile stress falling below the strength of the ice, halting crack propagation until a later time in which the cracking is re-initiated. The model requires three free parameters to recreate the cycloidal crack features: the crack initiation strength, the crack propagation strength, and the crack propagation speed. The parameters required by the model to produce the cracks imply either that the icy lithosphere is thin or weak [12], or that the background stress field is quite high. [8, 9]

Much of the evidence that could support the existence of non-synchronous rotation on Europa

comes from correlating models of crack formation to the observed distribution and orientation of surface cracks. In particular, the work of Hoppa and Greenberg has been used to try and reconstruct the background stress fields arising from non-synchronous rotation or polar wander, a concept discussed in the next section. The main idea with both of these is that if the ice shell is free to rotate with respect to the rest of the planet, immense stress fields can develop in the ice, and the form of these stress fields could be partially indicated by the distribution and shapes of surface cracks. [8,9] Their work has been used to suggest an non-synchronous rotation period between 50,000 years and 250,000 years. [9]

2.3 Polar Wander

Polar wander is a phenomenon in which the lithosphere of a body is displaced in latitude, independently of the body interior. On Europa, it is possible that the ice surface is decoupled from the core by the liquid ocean. In this case, if the inertia of the ice shell is sufficiently imbalanced, the entire shell could be made to move to align the maximum inertia with the planet's rotation axis. Work by Ojakangas and Stevenson explored the thermal equilibrium thickness of the ice shell on Europa, and the dynamics of a rigidly reorienting ice shell. [22,23] They determined that the shell may become dynamically unstable as it reaches thermal equilibrium, and could reorient by 90° about the satellite-planet direction on timescales much shorter than the timescale on which thermal equilibrium is achieved. The resulting process would be that the ice achieves thermal equilibrium over $\sim 10^7$ years, until it is critically imbalanced as the maximum and intermediate principal axes interchange, reorienting quickly to a dynamically favored orientation in $\leq 10^6$ years. This re-initializes the process, which will repeat in subsequent episodes of similar timescales. It is also possible that the whole ice shell drifts continuously on a timescale of $\sim 10^7$ years. [22,23]

2.4 Exogenic Modification of Surface Ice

Multiple authors have highlighted and studied the effects of the space environment on icy surfaces. Large-scale color patterns have been observed on the icy Galilean satellites and have been attributed to alteration by high-energy ions and electrons, [24] as well as sulfur ion implantation. [10,27] Past works have also extensively studied the interaction between jovian charged particles and the surface of Europa. [15] However, the modification of icy surfaces by charged particles is a phenomenon that is not unique to Europa. In particular, data from Cassini has provided a wealth of knowledge of similar processes affecting the Saturnian moons. In Schenk et al. [27], global high-resolution color maps of Saturn's icy satellites Mimas, Enceladus, Tethys, Dione, and Rhea were generated from Cassini data. A decrease in albedo across the trailing hemispheres of Tethys, Dione, and Rhea was noted, which also corresponded with an increase in infrared (IR) to ultraviolet (UV) ratio (redness). The authors noted that the longitudinal variation of the IR/UV ratio is fit well by a Gaussian centered at the antapex of orbital motion, whereas a weaker enhancement in the IR/UV ratio was found in the leading hemispheres, but was fit well by a sine curve. They speculated that its origin was different from that of the trailing hemisphere enhancements. Overall, the hemispheric albedo and color patterns were attributed to the combined effects of magnetospheric plasma bombardment, E-ring particles, small heliocentric impactors, and sub-micron dust particles. They note that particles smaller than about $0.05 \mu\text{m}$ in radius behave like ions in Saturn's magnetic field, and circle the planet faster than orbital velocity, overtaking the moons from behind. Larger particles such as dust grains $0.5 \mu\text{m}$ in radius orbit 1.5% faster than the Keplerian orbital velocity.

[11]

A detailed example of exogenic modification of surface ice can be found in Howett et al. [13] This work used data gathered from Tethys using Cassini’s Composite Infrared Spectrometer (CIRS) and Imaging Subsystem (ISS). It identified a thermal and color anomaly with warmer nighttime and cooler daytime temperatures, and a darker appearance in the IR/UV color ratio maps. The temperature anomaly indicates an increase in thermal inertia in low latitudes of the leading hemisphere. Ice thermal inertia is proportional to $\sqrt{k(1-p)}$, where k is the thermal conductivity, and p is porosity. The increase in thermal inertia inside the anomalous region indicates less porous and/or more thermally conductive surface ice than in the surrounding areas. [13] Because this anomaly is highly coincident with a region of high-energy electron bombardment, the authors concluded that the electrons alter the ice texture and make it more conductive than in the surrounding areas.

3 Europa’s Hemispheric Color Asymmetry

The hemispheric color asymmetry on Europa is a well-known feature in which the color on the leading hemisphere (in the direction of the orbital velocity vector) is generally not as dark as the trailing hemisphere. Work by Johnson et al. [16] constructed multispectral mosaics of Europa from the Voyager images. It was noted that the trailing hemisphere has lower relative UV spectral reflectance than the leading hemisphere, for which Io-related plasma impact was previously suggested as the cause. [19]

3.1 Albedo Data from Voyager

Previous work by Nelson et al. [20] took the Voyager global multispectral mosaic of Europa [16] and analyzed surface features with similar optical properties. In that work, the hemispheric asymmetry is highlighted in the ratio of ultraviolet to violet albedo, because the asymmetry becomes more intense with decreasing wavelength. The albedo ratio image also suppresses the effect due to color variations from individual surface features, revealing a smooth surface pattern of decreasing darkness as the cosine of the angle from the antapex of motion, or equivalently, a variation with the sine of the longitude in degrees East. The authors argue convincingly that this simple pattern is only consistent with an exogenic source, namely surface alteration by sulfur ion bombardment from the Jovian magnetosphere.

Johnson et al. [15] highlighted the effects of high-energy electrons and sulfur ions on low-temperature ices, and provided theoretical approximations of the longitudinal distribution of sulfur implantation on Europa’s surface. This result is reproduced in Figure 3. These results are characteristically similar to the sinusoidal variation seen in the ratio of ultraviolet to violet albedo in Nelson et al. This lends support to the idea that a sinusoidal variation in discoloration could be attributed to sinusoidal variation in intensity of the exogenic processes that produce the observed discoloration patterns.

In Nelson et al., the albedo in violet and ultraviolet was computed for fixed latitude for the whole range of longitude from the global multispectral mosaic, and the select results obtained are reproduced in Figure 4. The Ultraviolet/Violet curve shows the ratio of albedo in ultraviolet and violet, and is obtained from an average of $\pm 1^\circ$ latitude, and the Violet/Orange curve is for the single row of pixels along the equator. The lower half of the curve is also produced from a single row of

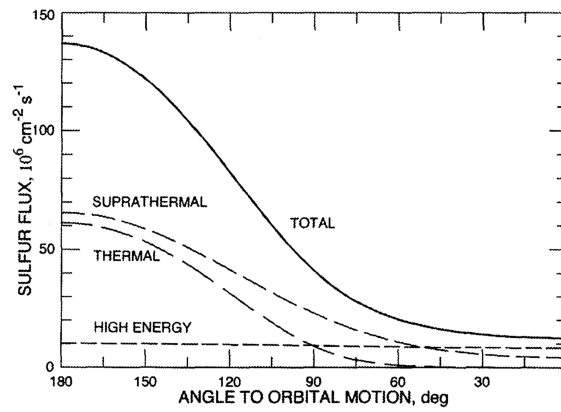


Figure 3: Theoretical Angular Distribution of Sulfur Implantation on Europa [15]

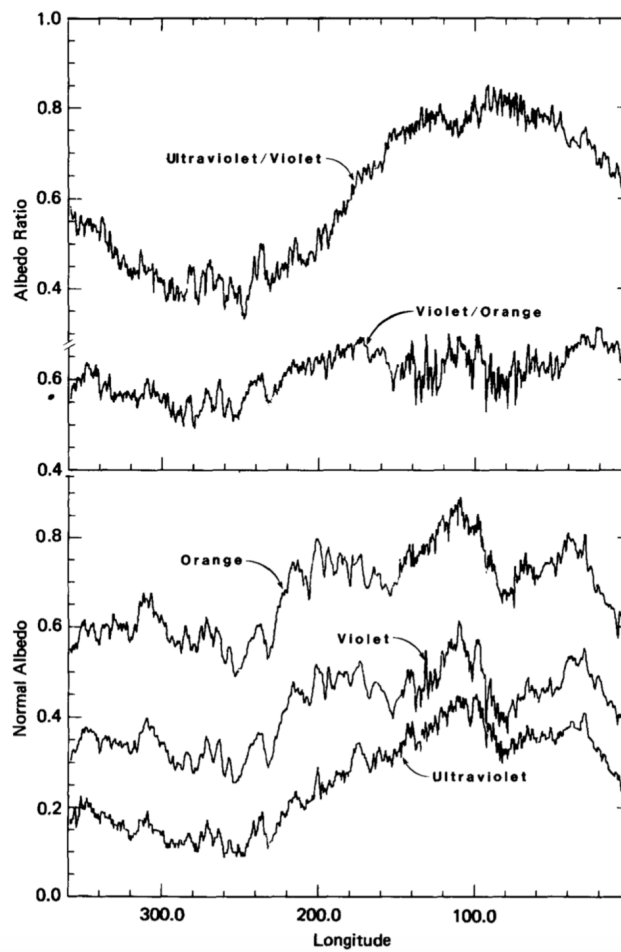


Figure 4: Europa Albedo vs. Longitude (deg. W) [20]

pixels along the equator. The violet to orange albedo ratio was shown to reflect geologic variations. The Ultraviolet/Violet curve shows a strong sinusoidal variation, which is also apparent in the global map of the ratio of ultraviolet to violet albedo, reproduced in Figure 5. In this figure, note that the faint streak traces remaining in the resultant image are caused by a slight misregistration

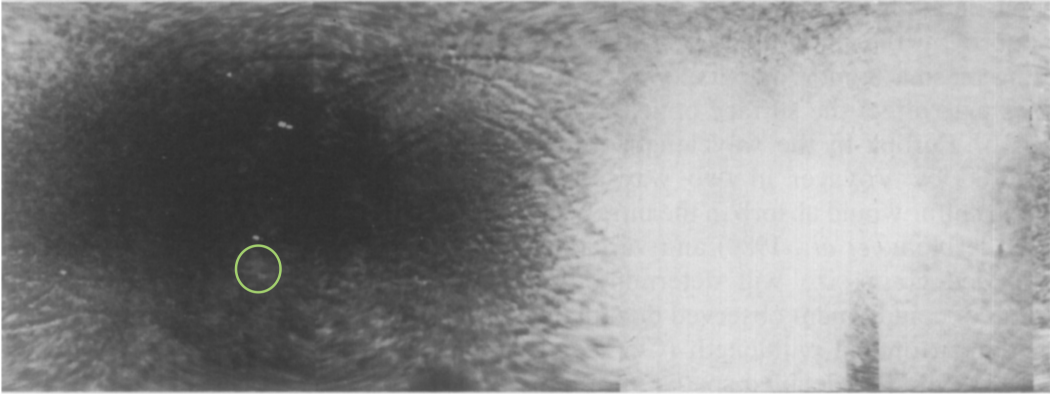


Figure 5: Europa Global Albedo Ratio Map [20]

between the two albedo images. [20]

The presence of a clear maximum and minimum in the ultraviolet to violet albedo ratio transect require either an ongoing process not yet completed, or a process that has settled into equilibrium. Nelson et al. argue that a completed process would produce a flatter top and bottom in the transect. Their hypothesis is that the global pattern is a result of the combined effects of sulfur ion implantation, micrometeorite gardening, and sputtering erosion – all of which are due to exogenic sources. [20]

3.2 Analytic Developments

With a $\sin \lambda$ variation in the albedo ratio due to a longitudinally sinusoidal variation in intensity of modification, one might expect that for a slowly rotating body, a Fourier decomposition of the longitudinal variations in albedo would reveal a signature of the rotation history as a non-negligible $\cos \lambda$ component – a remnant of discoloration in the past orientation. The following argument provides some analytical motivation for the existence of such a signature.

For any longitudinally varying optical parameter $r(\lambda)$ arising from the plasma bombardment depicted in Figure 6, a simple dynamic model is proposed, given in Eq. (3):

$$\dot{r}(\theta, a) = a (\sin \theta + 1) \quad (3)$$

where $\theta = \lambda + n^*t$ is the angular position of a spot on the surface on the equator, λ is the longitude in degrees east of the line towards Jupiter, and $n^* = 2\pi/T^*$ is the angular rate of any non-synchronous rotation. This establishes a relationship between the present longitude λ and its future angular measure, or equivalently, between the present longitude and its historical angular measure. For tidally locked synchronous rotation, $n^* = 0$. The term a is one-half of \dot{r} for a surface with normal vector $\hat{\mathbf{n}}$ satisfying $\hat{\mathbf{n}} \cdot \hat{\mathbf{u}} = -1$, where $\hat{\mathbf{u}}$ is the unit vector in the direction of Europa's velocity vector, or equivalently in the direction of the flow of the plasma.

The simple form of Eq. (3) is meant to serve as a simple first-order representation of a much more sophisticated process, which maximally affects the point on the equator facing the incoming plasma, and is assumed to not affect the surface directly opposite on the equator, 180 degrees to the east. Any discoloration of the surface by ion bombardment is assumed to be attributed to two main effects. First, as more ions are embedded in the icy surface, the optical properties of the surface

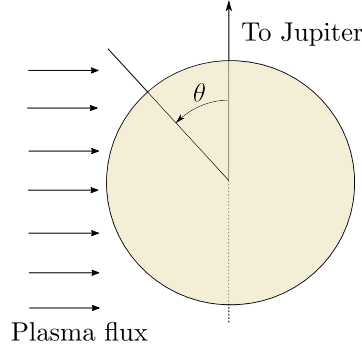


Figure 6: Europa Plasma Bombardment, Top View, $\theta = \lambda + n^*t$

will be increasingly influenced by the presence of this material. Second, any post-bombardment small-scale structural changes or chemical changes to the ice could also produce a change in optical properties. It seems reasonable that initially for a clean surface, the change in an optical property will appear nearly linear over the time scale of multiple orbits, if the ion flux is constant on average, and any resurfacing process is also constant on average. This explains why a is not considered to be a function of t or r in this analysis.

3.2.1 Analytic Model 1: Non-Saturating Discoloration Process

One assumption of the form of Eq. (3) is that the discoloration process is non-saturating, and there does not exist a maximum value of r . One would expect the surface could be maximally altered by the plasma bombardment, or some steady-state discoloration could be achieved. However, an initial investigation with this non-saturating model is still instructive.

Integrating Eq. (3), the following result is obtained:

$$r = at + c_1 - \frac{a}{n^*} \cos(\lambda + n^*t) \quad (4)$$

where c_1 is an integration constant that may be obtained by applying the initial condition at the initialization time $t \equiv 0$:

$$r(0) = r_0(\lambda) = c_1 - \frac{a}{n^*} \cos \lambda \rightarrow c_1 = \frac{a}{n^*} \cos \lambda + r_0(\lambda) \quad (5)$$

Substituting Eq. (5) into Eq. (4) and expanding:

$$r = r_0(\lambda) + at + \frac{a}{n^*} (\cos \lambda - \cos \lambda \cos(n^*t) + \sin \lambda \sin(n^*t)) \quad (6)$$

Expanding the time-dependent terms in the parentheses in their Taylor series up to $\mathcal{O}(n^{*2}t^2)$ and neglecting higher-order terms because n^* is small:

$$r \approx r_0(\lambda) + at + \frac{a}{n^*} \left(\cos \lambda - \cos \lambda \left(1 - \frac{n^{*2}t^2}{2} \right) + \sin \lambda (n^*t) \right) \quad (7)$$

Cancelling terms in Eq. (7) and simplifying, the final result is obtained:

$$r(\lambda, t) = r_0(\lambda) + a \left((1 + \sin \lambda) t + \frac{1}{2} t^2 n^* \cos \lambda \right) \quad (8)$$

As expected, Eq. (8) predicts that the non-synchronous rotation will produce a $\cos \lambda$ term in $r(\lambda, t)$. This equation will now be applied to a Fourier series fit of the albedo ratio data from Figure 4 to determine the unknown parameter n^* along with all other unknown parameters. The Fourier series fit is given in Eq. (9) where a_0 , a_1 , b_1 are the Fourier coefficients.

$$r = \frac{a_0}{2} + a_1 \cos \lambda + b_1 \sin \lambda \quad (9)$$

Applying the Fourier decomposition to the data, Figure 7 is produced. The values of the Fourier coefficients are $a_0 = 1.199586$, $a_1 = -2.63 \times 10^{-4}$, $b_1 = -0.210128$. Note the very small ratio a_1/b_1 . In the lowest frequency, the longitudinal distribution of the albedo ratio is almost entirely sinusoidal.

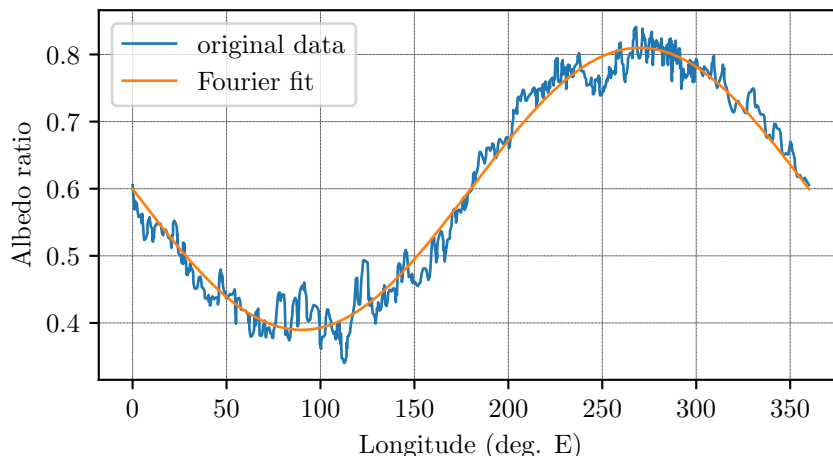


Figure 7: Fourier Series Fit of Albedo Ratio Data

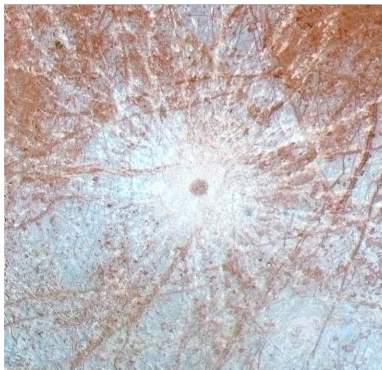


Figure 8: Pwyll Crater

Assuming $r_0(\lambda) \approx r_0 \forall \lambda$ (no large variations in the initial distribution $r_0(\lambda)$) and applying the

boundary conditions at $\lambda = 0, \pi/2, 3\pi/2$ to Eq. (8) and Eq. (9) and equating:

$$r(\lambda = 0) = r_0 + a \left(t + \frac{1}{2} t^2 n^* \right) = \frac{a_0}{2} + a_1 \quad (10a)$$

$$r(\lambda = \frac{\pi}{2}) = r_0 + 2at = \frac{a_0}{2} + b_1 \quad (10b)$$

$$r(\lambda = \frac{3\pi}{2}) = r_0 = \frac{a_0}{2} - b_1 \quad (10c)$$

$$r(\lambda = \pi) = r_0 + a \left(t - \frac{1}{2} t^2 n^* \right) = \frac{a_0}{2} - a_1 \quad (10d)$$

Eq. (10) has three unique expressions with four unknowns r_0, a, n^*, t , yielding the following ambiguous results:

$$r_0 = \frac{a_0}{2} - b_1 \quad (11a)$$

$$\eta = at = b_1 \quad (11b)$$

$$n^* t \sim 2 \frac{a_1}{b_1} \quad (11c)$$

However, estimating the timescale of formation t_P of the observed color asymmetry would resolve the ambiguity and enable the following order-of-magnitude estimate of n^* :

$$n^* \sim 2 \frac{a_1}{t_P b_1} \quad (12)$$

Pwyll crater, shown in Figure 8, can provide some constraint on the scale of t_P , because the albedo ratio of the more recently exposed icy ejecta has not returned to surrounding background levels (see the highlighted region in Figure 5). Using estimates of Pwyll's age [1] of $t_P \sim 10^6$ yr yields an approximate timescale of formation of the surface discoloration:

$$n^* \sim 2 \frac{a_1}{t_P b_1} = 10^{-9} \text{ rad/year} \rightarrow T^* \sim 10^9 \text{ years} \quad (13)$$

The estimate of $T^* \sim 10^9$ years suggests that there is no non-synchronous rotation and Europa is in fact tidally locked to Jupiter.

3.2.2 Analytic Model 2: Exponentially Saturating Discoloration Process

A slightly different approach to modeling the discoloration dynamics is useful, by highlighting the persistence of the important $n^* \cos \lambda$ term even for a saturating discoloration process, in which it is assumed that \dot{r} decays exponentially by some unknown global alteration decay parameter b :

$$\dot{r}(\theta, a) = a (\sin \theta + 1) e^{-bt} \quad (14)$$

Integrating Eq. (14), the following solution is obtained:

$$r = c_1 - \frac{ae^{-bt} (b^2 + n^2 + bn \cos(\lambda + n^*t) + b^2 \sin(\lambda + n^*t))}{b(b^2 + n^2)} \quad (15)$$

Applying the initial condition $r(0) = r_0(\lambda)$, the constant of integration c_1 is obtained:

$$c_1 = r_0(\lambda) + \frac{a(b^2 + n^2 + bn \cos \lambda + b^2 \sin \lambda)}{b(b^2 + n^2)} \quad (16)$$

Substitution of Eq. (16) into Eq. (15) yields the complete solution:

$$r = r_0(\lambda) + \frac{a(b^2 + n^2 + bn \cos \lambda + b^2 \sin \lambda) - ae^{-bt}(b^2 + n^2 + bn \cos(\lambda + n^*t) + b^2 \sin(\lambda + n^*t))}{b(b^2 + n^2)} \quad (17)$$

Expanding the time-dependent terms in the parentheses in their Taylor series up to $\mathcal{O}(n^{*2}t^2)$ and neglecting higher-order terms because n^* is small, the final expression $r(\lambda, t)$ is obtained:

$$r(\lambda, t) = r_0(\lambda) + \frac{a(b^2 + n^{*2} + bn^* \cos \lambda + b^2 \sin \lambda)}{b(b^2 + n^{*2})} - \frac{ae^{-bt}(b^2 + n^{*2} + b(n^* \cos \lambda + b \sin \lambda)(1 - \frac{1}{2}n^{*2}t^2) + bn^*t(b \cos \lambda - n^* \sin \lambda))}{b(b^2 + n^{*2})} \quad (18)$$

Applying the condition that the present-day distribution $r(\lambda)$ is expected to be in steady-state if it was generated by a saturating discoloration process, we let $e^{-bt} \rightarrow 0$, yielding the following highly simplified form for the present-day distribution:

$$r(\lambda) = r_0(\lambda) + \frac{a}{b} + \frac{a}{b^2 + n^{*2}}(n^* \cos \lambda + b \sin \lambda) \quad (19)$$

Next, applying the boundary conditions to Eq. (19):

$$r(\lambda = 0) = r_0 + \frac{a}{b} + \frac{an^*}{b^2 + n^{*2}} = \frac{a_0}{2} + a_1 \quad (20a)$$

$$r(\lambda = \frac{\pi}{2}) = r_0 + \frac{a}{b} + \frac{ab}{b^2 + n^{*2}} = \frac{a_0}{2} + b_1 \quad (20b)$$

$$r(\lambda = \frac{3\pi}{2}) = r_0 + \frac{a}{b} - \frac{ab}{b^2 + n^{*2}} = \frac{a_0}{2} - b_1 \quad (20c)$$

$$r(\lambda = \pi) = r_0 + \frac{a}{b} - \frac{an^*}{b^2 + n^{*2}} = \frac{a_0}{2} - a_1 \quad (20d)$$

Eq. (20) yields the following ambiguous but important expressions:

$$r_0 = \frac{a_0}{2} - \frac{a_1^2 + b_1^2}{b_1} \quad (21a)$$

$$a = \frac{b(a_1^2 + b_1^2)}{b_1} \quad (21b)$$

$$n^* = \left(\frac{a_1}{b_1}\right)b \quad (21c)$$

Again, the ambiguity may be resolved using Pwyll crater, but with a more accurate approach. The current r value of Pwyll crater, r_P , must be estimated from Figure 5, and we investigate a range of crater age estimates, [1] with $\lambda_P \approx 89^\circ$ E. From the albedo ratio map, it seems that Pwyll crater is nearly recovered to the same albedo ratio as the surrounding area, but not quite, so $r_P \approx 0.45$. Substituting this information and the Fourier coefficients and Eq. (21) into Eq. (18):

$$r_P \approx 0.81 + \frac{a(b^2 + n^{*2} + bn^* \cos \lambda_P + b^2 \sin \lambda_P)}{b(b^2 + n^{*2})} - \frac{ae^{-bt_P}(b^2 + n^{*2} + b(n^* \cos \lambda_P + b \sin \lambda_P)(1 - \frac{1}{2}n^{*2}t_P^2) + bn^*t_P(b \cos \lambda_P - n^* \sin \lambda_P))}{b(b^2 + n^{*2})} \quad (22)$$

Solving Eq. (22) numerically, we obtain $b \approx 6.5 \times 10^{-7}$ for $t_P = 3.0 \times 10^6$ years, and $b \approx 2.0 \times 10^{-6}$ for $t_P = 1.0 \times 10^6$ years. Both of these values are on the order of 10^{-6} . Thus, the scale of n^* is obtained:

$$n^* \sim \left(\frac{a_1}{b_1}\right) b \sim 10^{-9} \text{ rad/year} \rightarrow T^* \sim 10^9 \text{ years} \quad (23)$$

Interestingly and encouragingly, the estimate of $T^* \sim 10^9$ years agrees the first estimate from the model not accounting for saturation. This result again suggests that there is no non-synchronous rotation.

3.2.3 General Forms of Discoloration Models

All of the models explored in this work are of the following form:

$$\dot{r}(t) = a (\sin(\lambda + n^*t) + 1) f(t) \quad (24)$$

$$r(t) = \int_0^t a (\sin(\lambda + n^*\varphi) + 1) f(\varphi) d\varphi \quad (25)$$

The chief assumption of discoloration models of this form is that the saturation process, controlled by the form of $f(t)$, has no longitudinal dependency, while the discoloration rate at any one time is entirely dependent on the longitude at that time. Future work could explore how the form of $f(t)$ influences the analytic results, and how an introduction of longitudinal dependency to the saturation process $f(\lambda, t)$ affects the form of the solution $r(\lambda, t)$.

4 Discussion and Conclusions

Given that the hemispheric pattern of discoloration on Europa's icy surface is consistent with models of exogenic sulfur ion implantation [2], our results are readily explained if Europa's rotation has remained exactly synchronous with respect to the tidal bulge throughout its geologic history. Any departure from the synchronous state should manifest with a cosine signature in the Fourier decomposition of longitudinal distribution of discoloration, which we do not detect to within the measurement uncertainty. This effectively rules out all but the slowest rates of non-synchronous rotation. Even if our temporal calibration point, the crater Pwyll, is an order of magnitude older than published estimates (i.e., approaching the $\mathcal{O}(10^7)$ -yr mean crater retention age of Europa's surface), the period of non-synchronous rotation would be $> 10^8$ yr. True polar wander could effectively reset the longitudinal discoloration pattern, such that we cannot rule it out on timescales longer than the characteristic timescale for discoloration, which is $\sim 10^6 - 10^7$ yr, based on the analysis of Pwyll crater above.

This result is difficult to reconcile with earlier studies suggesting substantial reorientation with respect to the tidal bulge based on matching the induced stress field to observed fracture patterns [4, 18]. Those studies suggested at least 10's of degrees of non-synchronous rotation, which in our model would require time $t \sim T^*/10 \sim 10^8$ yr. An approximate Maxwell viscoelastic relaxation time of the lithospheric shell is $t_M = \eta/\mu \sim 10^3 - 10^4$ yr, with viscosity $\eta = 10^{21}$ Pa s and rigidity $\mu = 10^8 - 10^9$ Pa [14]. Therefore, we find $t_M/t \sim 10^{-5} - 10^{-4}$, such that lithospheric stresses induced by non-synchronous rotation cannot accumulate before relaxation occurs.

Our derived period of non-synchronous rotation exceeds Europa's surface age, and is therefore larger than the age of the tectonic features within the lithospheric region of the ice shell. Two different dynamic models of the discoloration process produced the same timescale conclusion. The present results constrain the asynchronous rotation period to be very long, if it exists, and especially rule out the previously suggested asynchronous rotation periods on the order of 10^4 - 10^5 years. This discrepancy refreshes the longstanding problem of linking modeled stresses to Europa's tectonic features, and further implies the decoupled ice shell possesses a significant permanent mass asymmetry in order to remain in the tidally locked state.

References

- [1] Edward B. Bierhaus, Clark R. Chapman, William J. Merline, Shawn M. Brooks, and Erik Asphaug. Pwyll Secondaries and Other Small Craters on Europa. *Icarus*, 153:264–276, 2001.
- [2] RW Carlson, MS Anderson, RE Johnson, MB Schulman, and AH Yavrouian. Sulfuric acid production on europa: The radiolysis of sulfur in water ice. *Icarus*, 157(2):456–463, 2002.
- [3] RW Carlson, WM Calvin, JB Dalton, GB Hansen, RL Hudson, RE Johnson, TB McCord, and MH Moore. Europa's surface composition. *Europa*, pages 283–327, 2009.
- [4] P. E. Geissler, R. Greenberg, G. Hoppa, P. Helfenstein, A. McEwen, R. Pappalardo, R. Tufts, M. Ockert-Bell, R. Sullivan, R. Greeley, M. J. S. Belton, T. Denk, B. Clark, J. Burns, J. Veverka, and the Galileo Imaging Team. Evidence for non-synchronous rotation of europa. *Nature*, 391(6665):368–370, 1998.
- [5] P. Goldreich. An explanation of the frequent occurrence of commensurable mean motions in the solar system. *Monthly Notices of the Royal Astronomical Society*, 130(3):159–181, Jan. 1965.
- [6] P. Goldreich and S. Peale. Resonant Spin States in the Solar System. *Nature*, 209:1078–1079, 1966.
- [7] Richard Greenberg, Paul Geissler, Gregory Hoppa, B Randall Tufts, Daniel D Durda, Robert Pappalardo, James W Head, Ronald Greeley, Robert Sullivan, and Michael H Carr. Tectonic processes on europa: Tidal stresses, mechanical response, and visible features. *Icarus*, 135(1):64–78, 1998.
- [8] Richard Greenberg, Gregory V. Hoppa, Gwen Bart, and Terry Hurford. Tidal Stress Patterns on Europa's Crust. *Celestial Mechanics and Dynamical Astronomy*, 87:171–188, 2003.
- [9] Richard Greenberg, Gregory V. Hoppa, Paul Geissler, Alyssa Sarid, and B. R. Tufts. The Rotation of Europa. *Celestial Mechanics and Dynamical Astronomy*, 83:35–47, 2002.
- [10] W. M. Grundy, B. J. Buratti, A. F. Cheng, J. P. Emery, A. Lunsford, W. B. McKinnon, J. M. Moore, S. F. Newman, C. B. Olkin, D. C. Reuter, P. M. Schenk, J. R. Spencer, S. A. Stern, H. B. Throop, and H. A. Weaver. New horizons mapping of europa and ganymede. *Science*, 318(5848):234–237, 2007.
- [11] Douglas P. Hamilton. Motion of Dust in a Planetary Magnetosphere: Orbit-Averaged Equations for Oblateness, Electromagnetic, and Radiation Forces with Application to Saturn's E Ring. *Icarus*, 101(2):244 – 264, 1993.

- [12] Gregory V. Hoppa, B. Randall Tufts, Richard Greenberg, and Paul E. Geissler. Formation of Cycloidal Features on Europa. *Science*, 285:1899 – 1902, September 1999.
- [13] C. J. A. Howett, J. R. Spencer, T. Hurford, A. Verbiscer, and M. Segura. Pacman returns: An electron-generated thermal anomaly on tethys. *Icarus*, 221:1084–1088, 2012.
- [14] Hermes M Jara-Oru e and Bert LA Vermeersen. Effects of low-viscous layers and a non-zero obliquity on surface stresses induced by diurnal tides and non-synchronous rotation: The case of europa. *Icarus*, 215(1):417–438, 2011.
- [15] R. E. Johnson, R. W. Carlson, J. F. Cooper, C. Paranicas, M. H. Moore, and M. C. Wong. *Radiation effects on the surfaces of the Galilean satellites*, volume 1, pages 485–512. 2004.
- [16] T. V. Johnson, L. A. Soderblum, J. A. Mosher, G. E. Danielson, A. F. Cook, and P. Kupferman. Global Multispectral Mosaics of the Icy Galilean Satellites. *J. Geophysical Research*, 88(B7):5789 – 5805, 1983.
- [17] Simon A. Kattenhorn. Nonsynchronous rotation evidence and fracture history in the bright plains region, europa. *Icarus*, 157(2):490 – 506, 2002.
- [18] Alfred S. McEwen. Exogenic and endogenic albedo and color patterns on europa. *Journal of Geophysical Research*, 91(B8):8077–8097, 1986.
- [19] D. Morrison and J. A. Burns. The jovian satellites. In *Jupiter: Studies of the interior, atmosphere, magnetosphere, and satellites*, pages 991–1034, Tucson, AZ, May 1975. University of Arizona Press.
- [20] Marcia L. Nelson, Thomas B. McCord, Roger N. Clark, Torrence V. Johnson, Dennis L. Matson, Joel A. Mosher, and Lawrence A. Soderblom. Europa: Characterization and Interpretation of Global Spectral Surface Units. *Icarus*, 65:129–151, 1986.
- [21] F Nimmo, PC Thomas, RT Pappalardo, and WB Moore. The global shape of europa: Constraints on lateral shell thickness variations. *Icarus*, 191(1):183–192, 2007.
- [22] Gregory W. Ojakangas and David J. Stevenson. Polar wander of an Ice Shell on Europa. *Icarus*, 81:242–270, 1989.
- [23] Gregory W. Ojakangas and David J. Stevenson. Thermal State of an Ice Shell on Europa. *Icarus*, 81:220–241, 1989.
- [24] C. Paranicas, J. F. Cooper, H. B. Garrett, R. E. Johnson, and S. J. Sturmer. *Europa’s Radiation Environment and Its Effects on the Surface*, page 529. 2009.
- [25] S. J. Peale. Origin and Evolution of the Natural Satellites. *Annual Review of Astronomy and Astrophysics*, 37(1):533–602, 1999.
- [26] Alyssa R. Sarid, Richard Greenberg, Gregory V. Hoppa, T. A. Hurford, B. R. Tufts, and Paul Geissler. Polar wander and surface convergence on Europa: Evidence from a survey of strike-slip displacement. *Icarus*, 158:24–41, 2002.
- [27] Paul Schenk, Douglas P. Hamilton, Robert E. Johnson, William B. McKinnon, Chris Paranicas, J urgen Schmidt, and Mark R. Showalter. Plasma, plumes and rings: Saturn system dynamics as recorded in global color patterns on its midsize icy satellites. *Icarus*, 211:740–757, 2011.